

Segregation and properties at curved vs straight $(000\bar{1})$ inversion boundaries in piezotronic ZnO bicrystals

Maximilian Trapp  | Peter Keil  | Till Frömling  | Jürgen Rödel |
Hans-Joachim Kleebe

Department of Materials and Earth Science, Technische Universität Darmstadt, Darmstadt, Germany

Correspondence

Maximilian Trapp, Department of Materials and Earth Science, Technische Universität Darmstadt, Alarich-Weiss Straße 2, 64287 Darmstadt, Germany.
Email: trapp@geo.tu-darmstadt.de

Funding information

Deutsche Forschungsgemeinschaft, Grant/Award Number: KL615/27-1 and RO954/28-1

Abstract

TEM and SEM investigations of ZnO bicrystal interfaces were undertaken with an aim to study the correlation of local grain-boundary structure, segregation, and electrical transport perpendicular to the interface. To this end, varistor-like ZnO bicrystals with piezotronic characteristics were chosen with $(000\bar{1}) \parallel (000\bar{1})$ tail-to-tail orientation with respect to the c-axis. In order to contrast different local grain-boundary structures with different coherency and segregation of bismuth, but identical macroscopic polarization state, two complementary processing techniques were applied. A diffusion-bonded bicrystal with an intermediate thin film containing Zn–Bi–Co–O provided a straight interface as reference. In contrast, a ZnO bicrystal prepared by epitaxial solid-state transformation was manufactured by bonding two ZnO single crystals with a 100 μm thick polycrystalline ZnO varistor material with a typical dopant composition including bismuth and cobalt. This structure was annealed to the point that a bicrystal was formed with the varistor concentration at the boundary, which was strongly curved due to the polycrystalline microstructure still providing a shadow image at the interface. The results highlight a distinct correlation between local interfacial morphology, degree of segregation of bismuth, and degree of non-linearity of the electrical transport across the interface.

KEYWORDS

bicrystal, interfaces, segregation, transmission electron microscopy, varistors, zinc oxide

1 | INTRODUCTION

Among various types of today's varistor ceramics, zinc oxide is one of the most commonly used materials due to its highly nonlinear current-voltage (I - V) characteristics.¹ The microscopic origin of the nonlinearity is attributed to electrostatic potential barriers at grain boundaries between individual ZnO grains, where charge carriers are trapped by dopant

induced defect states.^{2,3} Therefore, ZnO varistor ceramics are typically doped with bismuth or praseodymium. Both dopants are usually further combined with transition metal elements, such as manganese, cobalt, or nickel.¹ There is an implicit consensus in the literature that bismuth or praseodymium are needed in order to “activate” the grain boundaries, whereas the additional transition elements are necessary to improve the varistor performance.^{4–6} ZnO crystallizes

This is an open access article under the terms of the Creative Commons Attribution-NonCommercial-NoDerivs License, which permits use and distribution in any medium, provided the original work is properly cited, the use is non-commercial and no modifications or adaptations are made.

© 2019 The Authors. *Journal of the American Ceramic Society* published by Wiley Periodicals, Inc. on behalf of American Ceramic Society (ACERS)

in the noncentrosymmetric wurzite structure (*space group No.186* $P6_3mc$) and therefore has piezoelectric properties. Furthermore, with a band gap of 3.4 eV, ZnO is a wide-band gap semiconductor.⁷

While ZnO resistors are in a mature state of research, ZnO semiconductors entered center stage when their properties were coupled with its piezoelectricity in 2006. Wang et al⁸ utilized the combination of piezoelectric and semiconducting properties to tune electrostatic potential barriers at metal-ZnO Schottky junctions by applying mechanical stress to single crystalline ZnO nanowires. This has sparked research efforts for the development of new applications such as strain-triggered transistors, diodes or sensors.^{9,10} In a similar manner, double Schottky barriers at ZnO varistor grain boundaries can be manipulated by stress induced piezoelectric polarization charges.¹¹ These piezoelectric polarization charges increase or decrease the barrier height depending on the orientation of the polarization vectors and whether tensile or compressive stress is applied. The barrier height can be decreased almost entirely turning the ZnO–ZnO interfaces into a very sensitive and effective piezotronic system.^{11,12} In order to systematically study the influence of positive and negative piezoelectric polarization charges on varistor-type potential barriers, appropriately designed bicrystals provide a well-suited model system. As demonstrated in a previous publication,¹² ZnO bicrystal design by epitaxial solid-state transformation¹³ allows for both the precise alignment of the polarization vectors and the application of various doping strategies in order to optimize the piezoelectric response and define the electrostatic potential at the interface. The coupling of piezoelectricity, semiconducting properties, and varistor behavior at tailored ZnO bicrystal interfaces holds the potential for the development of novel multifunctional electronic devices.

To further increase the performance of such bicrystal devices, it is of great advantage to understand the potential barrier formation process at (0001) inversion boundaries. Therefore, the segregation behavior of varistor forming dopants such as Bi and Pr at such boundaries is of particular interest. In contrast with the transition element dopants commonly used, bismuth and praseodymium are virtually insoluble in ZnO,^{14,15} which can readily be explained by their much larger atomic and ionic radii compared to zinc. In consequence, they segregate to grain boundaries and triple junctions in polycrystalline ceramics.^{1,16–18} Besides the possibility to form secondary phases, these large dopants can substitute Zn atoms at grain boundaries, if special positions featuring sufficiently large Zn–O bond lengths are present providing wider spaces.^{19,20} Whereas these positions are a part of the periodically occurring structural units at coincidence site lattice (CSL) boundaries and likewise periodically arranged, they also appear in low-coherent, disordered interface configurations. In fact, Sato et al^{19,21} found the concentration of praseodymium at the boundary, as well as the nonlinear I - V behavior, to be

successively higher with decreasing coherency. Using the concept of coincidence reciprocal lattice points²² (CRLP), they designed Pr-Co-codoped bicrystals with $(8\bar{5}30) \parallel (11\bar{2}0)$ and $(2.11.\bar{1}3.0) \parallel (0001)$ orientation, which exhibited a minimized coherency at the interface. By showing the highest nonlinear I - V characteristics in a comparative study with samples of higher coherency,²¹ these bicrystals confirmed the relationship between coherency, dopant segregation, and varistor behavior. In consequence, grain-boundary coherency is a crucial parameter determining the electrostatic potential barrier in bicrystalline ZnO varistors.

Regarding piezotronic applications, the orientational degree of freedom is limited to (0001) inversion boundaries since it maximizes the amount of piezoelectric polarization charges that can be generated at the interface under the application of mechanical stress. In doing so, the c -axes can be aligned in either a Zn-polar head-to-head $(0001) \parallel (0001)$ or an O-polar tail-to-tail $(000\bar{1}) \parallel (000\bar{1})$ orientation. Since the descriptions “head-to-head” and “tail-to-tail” are inconsistently used in the ZnO literature, sometimes referring to c -axes and sometimes to the polarization vector, which has the reverse direction, we would like to point out that the terms “head-to-head” and “tail-to-tail” refer to the c -axis in this work. In the tail-to-tail orientation, compressive stress applied longitudinally to the c -axes will cause positive piezoelectric charges compensating negatively charged defect states at the boundary and hence decrease an existing potential barrier. In consequence, conductance will increase. In the head-to-head case, the effect will be the opposite with additional negative charges at the grain boundary, increasing the barrier height and lowering the conductance.

However, inversion boundaries free from any twist or tilt implicate a very coherent configuration according not only to the CRLP theory, but also to other approaches such as the low index planes of supercells (LIPS).^{23–25} The basic idea behind LIPS is that, in general, low indexed planes have a higher atomic density than higher indexed planes and hence are expected to provide more special arrangements if they are parallel to the boundary plane. For a perfect $(000\bar{1}) \parallel (000\bar{1})$ bicrystal, this is especially true. Notwithstanding the c -axis inversion, this configuration corresponds to a $\Sigma 1$ boundary and is hence closely related to a single crystal. In consequence, the formation of a varistor-type potential barrier, being a grain-boundary phenomenon, appears to be highly unlikely for such bicrystals. Nevertheless, not only an obvious bismuth segregation to the interface, but also a significant nonlinear I - V response was observed in the respective samples from our previous study.¹² Although the main reason for this counterintuitive behavior is expected to be the consequence of the special synthesis process used, ie the epitaxial solid-state transformation, it has not been clarified in detail yet. Therefore, the respective bicrystal configuration was comprehensively investigated by scanning and transmission

electron microscopy (SEM/TEM) and compared to a reference sample of identical orientation but different synthesis method. The main focus of this study is the bismuth segregation and the corresponding driving forces.

2 | EXPERIMENTAL PROCEDURE

Two types of ZnO bicrystals were prepared for the TEM investigation. Referring to their respective synthesis method, which are epitaxial solid-state transformation (EST) and diffusion bonding (DB), the samples are termed EST- and DB-sample in the following. For the EST-bicrystal, a doped polycrystalline ZnO ceramic (PC) of 100 μm thickness is placed between two 5 mm \times 5 mm \times 0.5 mm ZnO single crystals (SC), which are in tail-to-tail orientation of the c -axis. Under a load of 1.5 MPa, the sample is diffusion bonded at 1100°C for 2 hours in air in order to achieve a well-bonded SC–PC–SC stack. Subsequently, the stack is annealed at 1100°C for 65 hours to promote grain growth of the single crystals into the polycrystalline layer until the latter is consumed completely. In consequence, a doped $(000\bar{1})\parallel(000\bar{1})$ ZnO bicrystal with a single grain boundary is formed. Doping is controlled by the composition of the polycrystalline sacrificial layer, which was 97.27ZnO; 0.6Bi₂O₃; 0.63Co₃O₄; 0.55Mn(C₅H₇O₂)₂; 0.35Cr₂O₃; 0.6NiO (all values in mol%). A detailed description of the bicrystal preparation process by epitaxial solid-state transformation can be found in a previous publication.¹²

In contrast, the DB-bicrystal is synthesized by directly hot pressing two ZnO single crystals in tail-to-tail orientation at 1000°C for 1 hour under a load of 1.5 MPa. Doping is achieved by depositing a Zn–Bi–Co–O film of approximately 75 nm thickness on the $(000\bar{1})$ surface of one of the single crystals by RF magnetron sputtering prior to bonding. The composition of the sputtering target was 90 mol% ZnO, 5 mol% Bi₂O₃ and 5 mol% Co₃O₄.

For TEM investigations, thin foil cross sections of both bicrystals were cut out in $[\bar{1}2\bar{1}0]$ and $[01\bar{1}0]$ directions and polished down to a thickness of 10 μm using an Allied MultiPrep polishing system (Allied High Tech Products Inc) with diamond lapping films of grain sizes from 15 μm down to 0.1 μm . Subsequently, the samples were mounted on supporting molybdenum TEM grids (100 mesh; Plano) and argon ion-milled using a DuoMill 600 (Gatan) until electron transparency of the interface regions was reached. In doing so, low acceleration voltages of 4 kV were applied in order to avoid the unintended removal of possibly present amorphous interface films as reported by Chiang et al²⁶ for polycrystalline ZnO varistor ceramics. An additional $[01\bar{1}0]$ cross section of the EST-bicrystal was surface polished and lightly carbon coated (Med 010, Balzers Union, Balzers, Liechtenstein) for SEM investigations, whereas the

TEM sample was also used for the SEM study in case of the DB-bicrystal. TEM investigations were performed on a JEOL JEM 2100F and a C_s -corrected JEOL JEM ARM 200F (JEOL) both equipped with an energy-dispersive spectroscopy (EDS) system (JEM 2100F: TEM 250 SDD, Oxford Instruments; ARM 200F: JED 2300T, JEOL). The SEM used is a JEOL JSM 7600F (JEOL). For HAADF-STEM imaging, a camera length of 6 cm was used, which corresponds to an inner and outer detector acceptance angle of 90 mrad and 174.5 mrad, respectively. The presented EDS point measurements were performed using a C_s -corrected probe with a beam current of 68 pA for a lifetime of 150 seconds under application of a drift-correction software (Analysis Station 3.8.0.30, JEOL).

For electrical measurements, Al/Au-based ohmic contacts were deposited on the two outer surfaces of the bicrystals. I - V measurements were performed using a source measurement unit (Keithley 2450, Keithley Instruments Inc) in a voltage range between 0.1 and 10 V, while the current output was limited to 100 mA.

3 | RESULTS AND DISCUSSION

3.1 | ZnO bicrystal—prepared by epitaxial solid-state transformation (EST)

SEM investigations of the interface of the ZnO bicrystal prepared by epitaxial solid-state transformation revealed a meandering grain boundary as depicted in Figure 1A. No indications for intergranular films were found in the SEM. However, secondary oxide phases of dopant elements are incorporated in the bulk as remnants of the former polycrystalline layer. HR-TEM imaging confirms that no crystalline or amorphous film exists at the bicrystal boundary by featuring an atomically bonded interface (Figure 1B). The single crystallinity of both ZnO bicrystal halves was verified by electron diffraction in the TEM as illustrated by the SAED insets. A small mismatch of about 1° twist and 1° tilt, which equals a rotation around the c - and the a -axis, respectively, was determined from the deviation of the $[\bar{1}100]$ zone axis on both sides of the interface.

Two-beam bright-field imaging using a small objective aperture (5 μm) exhibited strong periodic contrast variations at the interface, which is indicative for local strain (Figure 2A). Furthermore, higher magnified STEM imaging of the same region revealed a dislocation network along the boundary with typical fish scale-like contrast (Figure 2B).

Since the intensity in HAADF-STEM is proportional to the square of the atomic number Z , the spots in Figure 3A, which are significantly brighter than the nearby background, indicate the presence of bismuth atoms within the dislocation network. For clarification it should be noted that only the upper crystal is in perfect zone-axis orientation due to the tilt and twist between the bicrystal halves. In consequence,

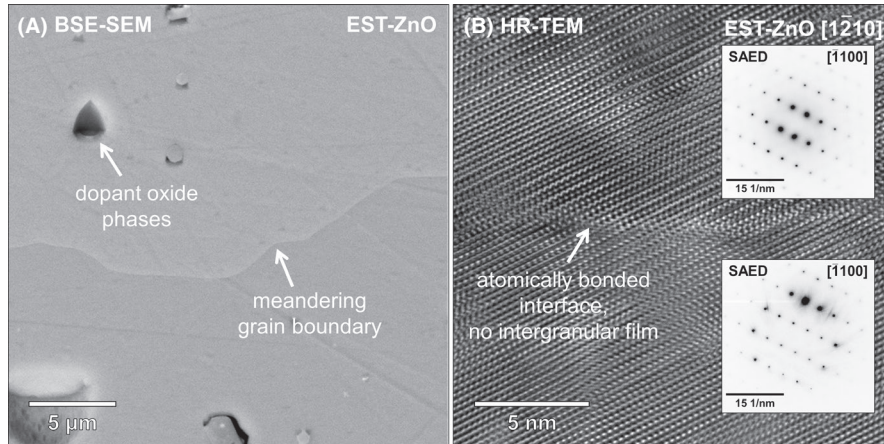


FIGURE 1 A, BSE-SEM image highlighting the formation of a meandering grain boundary with locally varying curvature. Grains of dopant oxides, which are remnants from the former polycrystalline layer, are incorporated in the bulk as secondary phases. B, HR-TEM imaging reveals an atomically bonded interface, which is free from any crystalline or amorphous intergranular film. The SAED insets depict a slightly misaligned zone axis for the lower crystal due to a mismatch of about 1° tilt and 1° twist

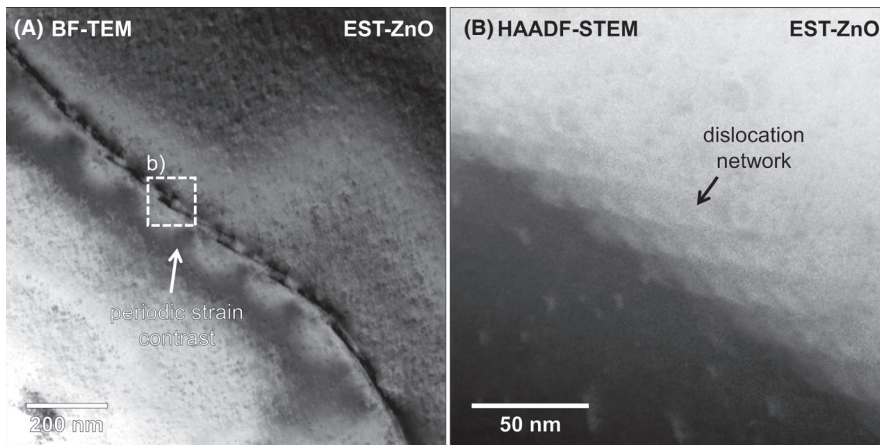


FIGURE 2 A, Two-beam bright field image displaying periodic strain contrast along the curved grain boundary. B, HAADF-STEM reveals a network of grain-boundary dislocations at the interface. The grain boundary is tilted in this image for the purpose of a better depiction of the characteristic fish scale-like contrast

electron channeling in the oriented crystal causes a higher intensity for the Zn atomic columns in relation to unoriented or disordered regions at the grain boundary or in the opposed crystal.^{27,28} However, this does not represent a chemical difference. Atomically resolved EDS point measurements (Figure 3B) verify this finding and further demonstrate that the incorporation of bismuth is extremely localized. Bismuth was only found in the immediate vicinity of the interface, an area approximately <2 nm wide, whereas the ZnO bulk appears to be free from any bismuth, even if the measurements are carried out in a distance of less than 10 atomic layers from the boundary. A quantification of the EDS data yields a local bismuth concentration of 1.8 mol%. The minimum mass fraction (MMF) of bismuth in ZnO, representing its detection limit for the presented EDS measurements is $c_{\text{Bi}}(\text{MMF}) = 2.17 \text{ wt}\% = 0.86 \text{ mol}\%$, derived from the determined Bi concentration (1.8 mol%) and the corresponding peak (I_{Bi}) to background (I_{Bi}^b) ratio of the Bi-L α line using Equation (1).²⁹

$$c_{\text{Bi}}(\text{MMF}) = 3 \sqrt{2 \cdot I_{\text{Bi}}^b \cdot c_{\text{Bi}} / (I_{\text{Bi}} - I_{\text{Bi}}^b)} \quad (1)$$

Due to the fact that no distinct Bi-phases were observed at the interface, the results strongly suggest that bismuth is incorporated on appropriate ZnO lattice sites in close vicinity to the dislocation cores. Other dopants like Cr, Mn, Co, and Ni form solid-solutions with ZnO^{30,31} and hence are found in both the bulk and at the interface. No indications were found for a segregation or an enrichment at the grain boundary. The Mo and Cu peaks originate from the supporting TEM grid and the sample holder respectively.

3.2 | ZnO bicrystal—prepared by sputtering & diffusion bonding (DB)

In contrast with the EST-bicrystal, the grain boundary of the diffusion bonded sample is comparably flat and uniform as depicted by the SEM image in Figure 4A. However, Bi-rich inclusions are found at the interface. The crater-like surface structures in the vicinity of the grain boundary are preparation artifacts due to ion-milling. Electron diffraction measurements

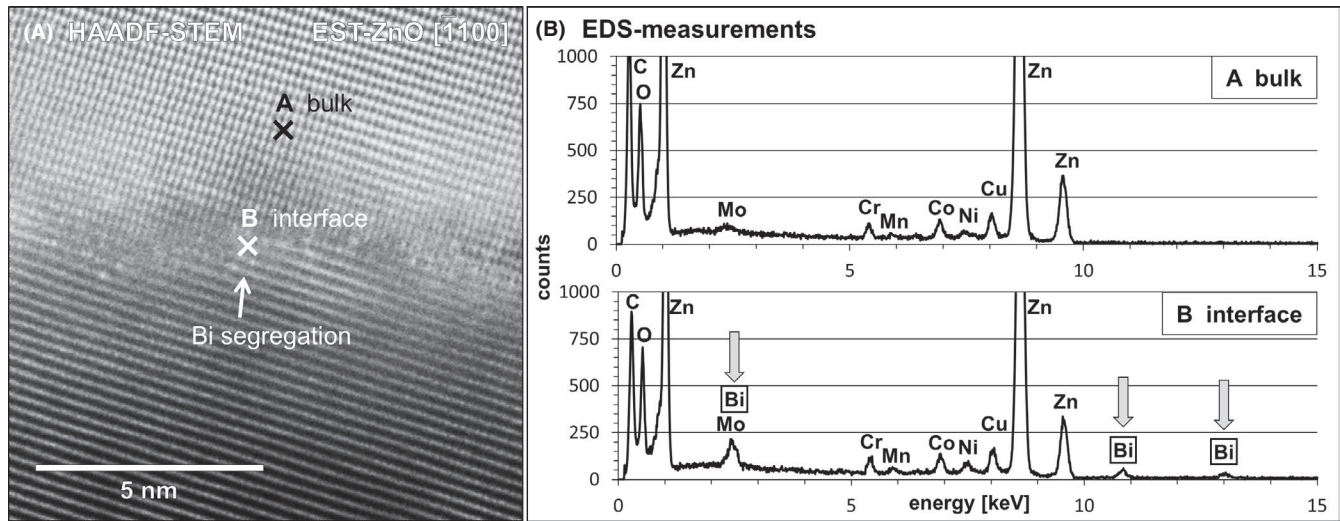
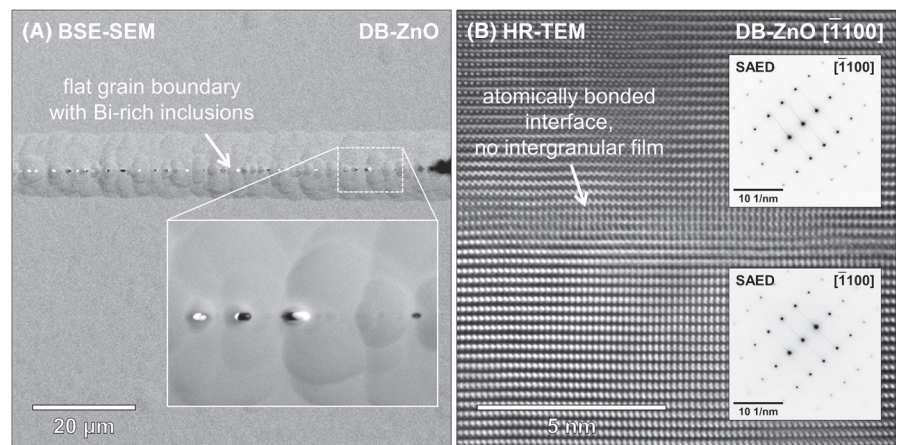


FIGURE 3 A, Atomically resolved HAADF-STEM reveals a distinct segregation of Bi atoms at the dislocation network. Due to twist and tilt between the bicrystal halves, only the upper crystal is in perfect zone-axis condition. In consequence of electron channeling effects, atomic columns appear brighter in this region. This does not indicate chemical differences, whereas the individual spots at the interface remain indicative for bismuth as they are significantly brighter than the nearby background. B, EDS measurements verifying that bismuth is only present directly at the grain boundary, whereas the other dopants Cr, Mn, Co, and Ni are found in both the bulk and at the interface. The Mo and Cu peaks originate from the supporting grid and the sample holder respectively

FIGURE 4 A, BSE-SEM image reveals a straight interface in the DB-bicrystal. Bi-rich inclusions are located at the grain boundary. The crater-like structures in the vicinity of the interface are ion-milling artefacts. B, HR-TEM image of the grain boundary showing an atomically bonded interface free from crystalline or amorphous intergranular films. No twist or tilt is detected by electron diffraction measurements (SAED insets)



of the $[1\bar{1}00]$ zone axes orientations reveal that the bicrystal is virtually free from any twist or tilt (SAED images in Figure 4B). HR-TEM imaging features an atomically bonded interface free from crystalline or amorphous films (Figure 4B).

As detailed in Figure 5, the precipitates are δ - Bi_2O_3 grains with a size of 40–200 nm and characteristically large dihedral angles θ in the range of 140° at triple junctions along the bicrystal interface. The identification of the face-centered-cubic fluorite structure of δ - Bi_2O_3 is supported by the observation of superlattice reflections, which are characteristic for this anion-defective modification.^{32,33} Given that undoped δ - Bi_2O_3 itself contains vacant anion sites, it remains unclear if this superlattice formation is due to a dopant independent ordering of vacancies or due to impurities. In any case, dopants that are typically related to the formation of such superstructures, ie metal ions with higher valences,³² were not added

in the synthesis or detected in EDS measurements. Regarding the segregation behavior of bismuth, the δ -phase is known to exhibit poor wetting properties of ZnO grain boundaries as compared to the low temperature α -phase.³⁴ This is not only consistent with the observed large dihedral angles $\theta \gg 60^\circ$, which indicate de-wetting and restriction of the Bi-phase from the interface,³⁵ but also with a closer investigation of the interface sections between the individual δ - Bi_2O_3 grains, revealing that these segments are apparently free from any bismuth.

Neither HAADF-STEM imaging, nor EDS measurements indicate a segregation or incorporation of Bi in these regions (Figure 6). In addition, the atomically resolved images reveal a highly coherent grain boundary with a low defect concentration and only minor lattice distortions. Nevertheless, atom columns at the grain boundary exhibit a significantly lower intensity compared to the bulk regions

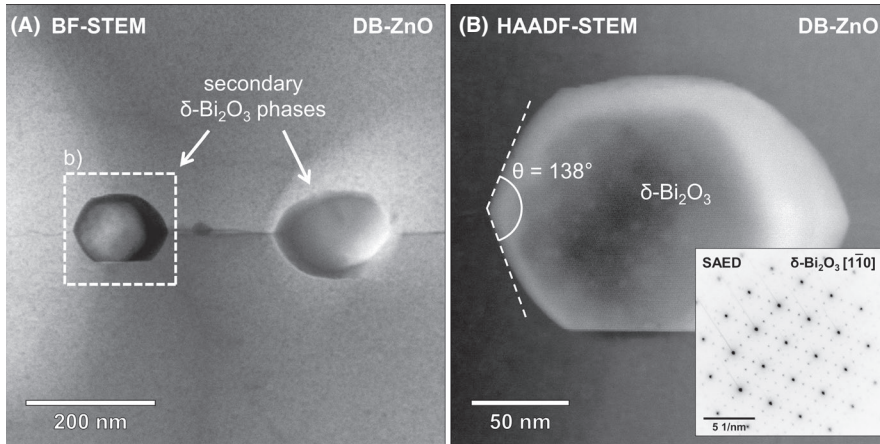


FIGURE 5 A, BF-STEM image of the interface depicting a predominantly straight grain boundary with δ - Bi_2O_3 crystallites of 40–200 nm size. B, Higher magnified HAADF-STEM image of a bismuth oxide crystallite. The SAED image indicates fcc δ - Bi_2O_3 , which is supported by the occurrence of characteristic superlattice reflections. Large dihedral angles θ , which indicate non-wetting behavior, are typical for the δ - Bi_2O_3 inclusions

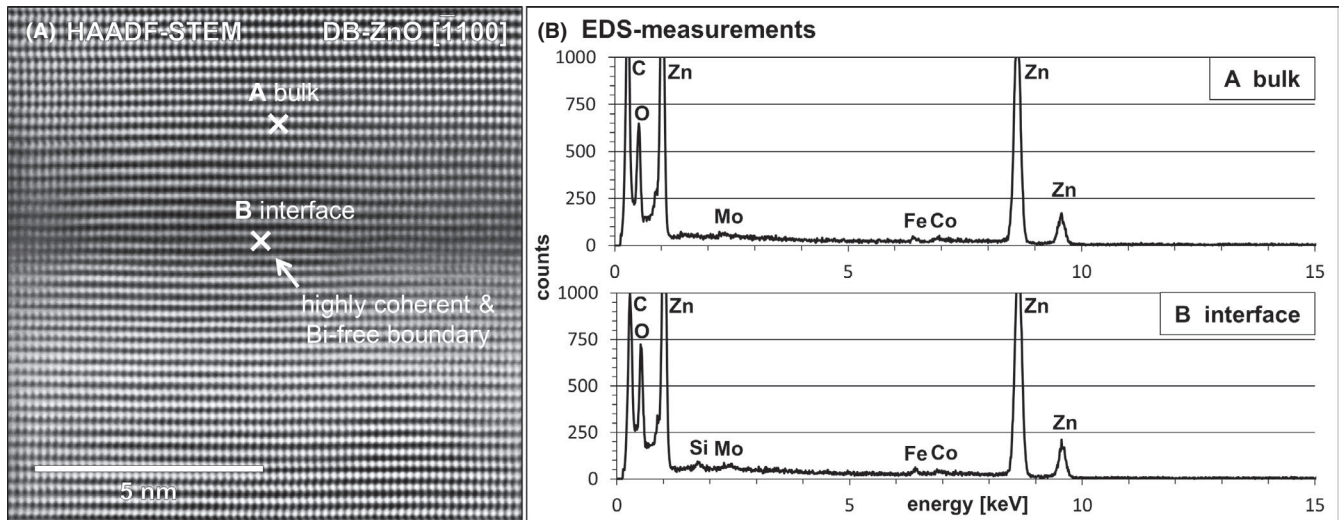


FIGURE 6 A, HAADF-STEM image verifying that the grain boundary between the individual δ - Bi_2O_3 grains is highly coherent and predominantly defect free. Furthermore, no indications for bismuth were observed in the image or in the corresponding EDS measurements (B). The lower intensity of the atomic columns at the boundary is attributed to electron de-channeling effects by a minor lattice distortion and a partial substitution of Zn by Si. The Si enrichment at the boundary most likely originates from a surface contamination prior to bonding

in the HAADF image. Besides the effect of electron de-channeling due to minor lattice distortions, this observation can also be explained by a minor contamination with silicon, which was detected by the EDS measurements at the interface (Figure 6). Since Si most likely substitutes Zn in ZnO^{36} and its atomic number is significantly lower, the respective region would create less intensity in HAADF-STEM imaging. The origin of the silicon is attributed to a contamination of the single crystals prior to diffusion bonding.

3.3 | Segregation behavior of bismuth

Both ZnO bicrystals have in principle the same $(000\bar{1}) \parallel (000\bar{1})$ orientation, ie a tail-to-tail inversion boundary. Hence, both are expected to exhibit a highly coherent grain boundary and a similar segregation behavior of bismuth.

However, some significant differences were observed. The bismuth in the EST-bicrystal originates from Bi_2O_3 phases in the polycrystalline layer and then distributes at the interface, which is formed during the epitaxial grain growth. Neither Bi-free interface sections, nor any connection of the Bi incorporation to secondary phase formation were observed (Figure 7A). On the contrary, the DB-bicrystal starts with a continuous dopant layer at the interface, which then disintegrates upon the annealing step. While cobalt forms a solid solution in the ZnO lattice, bismuth accumulates and forms a nonwetting secondary δ - Bi_2O_3 phase (Figure 7B). The actual bicrystal interface of the DB-sample is coherent and bismuth free. Hence, little to no varistor behavior is expected, which is confirmed by the electrical measurements (Figure 8B). In contrast with that, the meandering grain boundary in the EST-bicrystal is locally strongly curved, hence much less coherent and has a notable amount of bismuth incorporated at the interface,

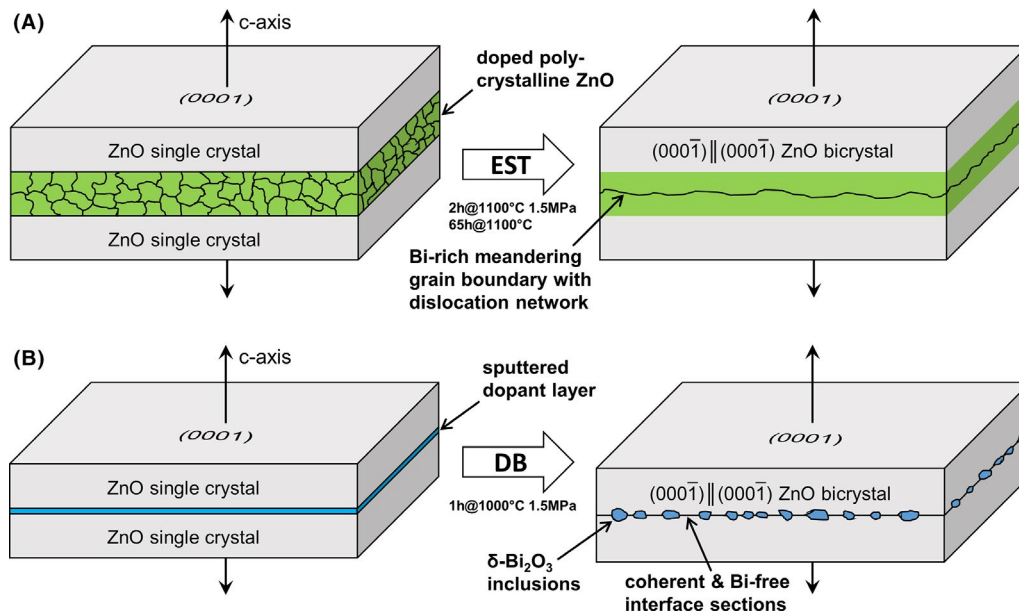


FIGURE 7 Illustration of the different bismuth segregation behavior in the two ZnO bicrystals prepared by (A) epitaxial solid-state transformation (EST) and (B) diffusion bonding (DB). A low-coherent meandering grain boundary with a bismuth incorporating dislocation network is formed in the EST-bicrystal (A). In the DB-bicrystal (B), bismuth accumulates to nonwetting δ - Bi_2O_3 inclusions with highly coherent and Bi-free interface sections in between [Color figure can be viewed at wileyonlinelibrary.com]

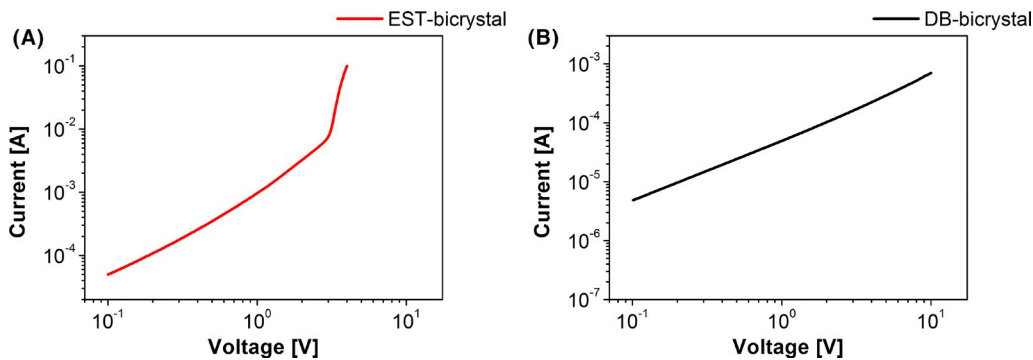


FIGURE 8 I - V characteristics of (A) the ZnO bicrystal synthesized by epitaxial solid-state transformation and (B) the diffusion bonded bicrystal. Whereas the EST-sample clearly exhibits nonlinear characteristics with a coefficient of $\alpha \approx 11$, the DB-bicrystal is characterized by an almost ideal ohmic behavior ($\alpha \approx 1$) [Color figure can be viewed at wileyonlinelibrary.com]

which correlates well with the distinctively observed non-linearity in the I - V plot (Figure 8A).

The continuous dislocation network at this interface is suggested to be the main mechanism retaining bismuth at the EST-bicrystal interface. The comparably large quantity of local structural defects and corresponding lattice distortions provides special positions with excess free volume sufficient for the stable incorporation of large bismuth ions. The DB-bicrystal features the inverse relationship by exhibiting a quasi defect-free grain boundary with no bismuth segregation. A comparison regarding the duration of the annealing steps indicates the stability and permanence of the bismuth doping, since the sputtered dopant layer is already withdrawn from the interface after only 1 hour, whereas the dislocation network and the incorporated

bismuth are still present after 65 hour of annealing. Furthermore, this observation correlates well with the stability of comparable impurity-decorated dislocation networks reported for polycrystalline Cu-doped ZnO.³⁷ We propose the formation of the dislocation network being a consequence of the synthesis method. During epitaxial solid-state transformation, the fronts of the opposing single crystals grow towards each other until complete consumption of the intermediate doped polycrystalline ZnO layer. Regarding the growth rates, this process is not completely uniform along the progressing boundaries, considering that different sizes and orientations of ZnO crystals are present as well as the various secondary phases. In consequence, a 3-D meandering grain boundary is formed in the final step, since the single crystalline fronts encounter

each other at different positions and angles. Due to the local curvature and the observed mismatch between the bicrystal halves, grain-boundary dislocations are formed, which constitute the observed dislocation network at the interface.

With respect to the observation that neither crystalline nor amorphous intergranular films were formed, the observed nonlinearity indicates that these are not essential for the creation of the necessary defect states and are also not an equilibrium grain-boundary state in the case of bicrystalline ZnO. These findings differ from earlier reports on ZnO ceramics showing that amorphous Bi-containing phases at grain boundaries are beneficial or even responsible for good varistor properties.^{26,38} However, the presence or absence of such films might be the consequence of the synthesis conditions and the different poly- and bicrystalline nature. It is also noteworthy that both cases are consistent with the general model of potential barrier formation, which just presupposes “grain-boundary material” including defect states but not necessarily intergranular films.^{1,39}

3.4 | *I-V* characterization

As displayed in Figure 8, the differently prepared bicrystals exhibit substantially different electrical characteristics. A distinct varistor behavior is observed for the EST-bicrystal with a nonlinear coefficient of $\alpha \approx 11$ in the breakdown region at 3.25 V. On the contrary, the *I-V* characterization of the DB-bicrystal features an approximately linear trend ($\alpha \approx 1$), which corresponds to almost ideal ohmic properties and hence indicates the absence of a varistor-like potential barrier at the interface. The onset of the breakdown region at 3.25 V in the EST-bicrystal is in agreement with the expected voltage for a single “active” grain boundary in ZnO.^{1,40} Since the overall breakdown voltage scales with the number of active grain boundaries,¹ these results indicate that additional phase boundaries between ZnO and secondary oxide grains in the bulk or at the interface either do not measurably affect the *I-V* characterization or are not included in the current path. Therefore, the overall electrical response is regarded to be determined by the electrical properties only of those bicrystal interface sections, which are free of secondary phases, since they represent the actual single ZnO–ZnO boundary.

3.5 | Thermodynamic aspects of Bi segregation at ZnO grain boundaries

A qualitative understanding of the thermodynamic aspects of the observed Bi segregation can be attained by applying Gibbs adsorption isotherm⁴¹ as provided in Equations

(2) and (3) for the straight and the curved interface, respectively.

$$d\gamma (\text{straight}) = -\Gamma_{\text{sat}(\text{straight})} d\mu (\text{straight}) \quad (2)$$

$$d\gamma (\text{curved}) = -\Gamma_{\text{sat}(\text{curved})} d\mu (\text{curved}) \quad (3)$$

These equations provide the change of interfacial energy, $d\gamma$, as a function of interfacial excess of segregating species (here bismuth), Γ_{sat} , and the change of chemical potential of that species, $d\mu$. In general, the anisotropy of segregation depends on five macroscopic degrees of freedom including the orientation of bulk phases as well as the relative orientation of the interface with respect to these.⁴² Hence, a general discussion quickly becomes intractable and case-specific. Our experimental approach, in contrast, fixes the orientation of the bulk materials at both sides of the interface. The grain-boundary orientation takes on two extremes. On the one hand, it is fixed by the orientation of the prior interface for the DB bicrystal resulting in a perfectly straight interface. On the other hand, it renders maximum local variation with respect to all three grain-boundary angles for the EST bicrystal due to the 3-D meandering interface, which is the consequence of the random microstructure of the sacrificial polycrystalline layer.

Segregation in general requires consideration of the solute concentration in the bulk to include the variation in configurational entropy if the solute atoms diffuse from bulk to interface.^{42,43} However, as bismuth is virtually insoluble in ZnO—as described in the introduction—solid solution of bismuth in the bulk ZnO can be neglected. In our case, bismuth is considered as available in a quasi-infinite reservoir. For the case of the DB bicrystal, this reservoir is formed by grain-boundary precipitates (Figure 5). It is provided by bulk precipitates for the EST bicrystal,¹² formed during grain growth of the single crystal by separating from the grain boundary.

Therefore, our experimental approach combines the two extreme cases of straight vs curved interface of identical average orientation with the simple case of segregation where an infinite source feeds the segregating species without interference of a bulk solute. Hence, the very simple Equations (2) and (3) suffice. From our experimental result we obtain that for the case of the straight interface (Equations 2) segregation does not occur and the bismuth interfacial excess, $\Gamma_{\text{sat}(\text{straight})}$, is equal to zero. For the case of the curved interface, the segregation is strongly promoted due to the lower grain-boundary coherency.¹⁹ This high degree of segregation is reflected by the TEM evidence (Figure 3) and the large nonlinearity factor of $\alpha \approx 11$. This large nonlinearity is consistent with the factor of $\alpha > 20$ for an interface with minimal coherency, which did not provide macroscopically a tail-to-tail orientation.²¹

For the case of the curved interface, grain-boundary reconstruction is likely to occur. This reconstruction typically includes the formation of dislocations, steps, and terraces, which encompass excess free volume promoting the incorporation of segregating atoms. Upon segregation, the bismuth atoms lower the interfacial energy, γ , by decorating the meandering interface of the EST-bicrystal (Figures 2 and 3). In contrast, no further reduction in the total free energy is possible in the DB-bicrystal due to the already low-energy state of the interface and the lack of dislocations and excess free volume. There is a large volume fraction of bismuth in the form of secondary phase, ie δ -Bi₂O₃ available, but no bismuth was found to segregate.

Furthermore, the dihedral angles θ of δ -Bi₂O₃ at the grain boundary (Figure 5), ie at triple junctions with ZnO, depend on the free energy γ of ZnO/ZnO in relation to ZnO/ δ -Bi₂O₃ interfaces and hence can be used to estimate the relative energies of the DB-bicrystal interface with and without wetting using Equation (4):

$$\begin{aligned} \gamma(\text{ZnO/ZnO})/2\gamma(\text{ZnO/Bi}_2\text{O}_3) &= \cos(\theta/2) \Leftrightarrow \gamma(\text{ZnO/Bi}_2\text{O}_3) \\ &= \gamma(\text{ZnO/ZnO})/2\cos(\theta/2) \end{aligned} \quad (4)$$

With a dihedral angle $\theta = 138^\circ$ and taking into account that two ZnO/Bi₂O₃ interfaces are present in case of a wetted grain boundary, Equation (4) yields $2\gamma(\text{ZnO/Bi}_2\text{O}_3) = 2.8\gamma(\text{ZnO/ZnO})$. This result does not only confirm the low-energy state of the nonwetted DB-bicrystal interface, it is also consistent with the described necessity of an increased interfacial energy, eg by the introduction of curvature, defects, mismatch, etc, in order to provide a sufficient segregation potential as in the EST-bicrystal. With respect to the high sintering temperatures during bonding and annealing bismuth is rendered highly mobile,⁴⁴ any kinetic constraints preventing a segregation determined by thermodynamic equilibrium are excluded. In consequence, the straight interface is devoid of any nonlinearity ($\alpha \approx 1$), as demonstrated in Figure 8B. This is consistent with the work by Sato et al¹⁹ on Pr-Co doped (0001) || (000 $\bar{1}$) bicrystals, which exhibited a comparably straight and highly coherent interface without any detectable Pr segregation and quasi-linear characteristics ($\alpha_{\text{max}} = 1.2$).

The observed anisotropy of segregation is similar to examples described in the relevant literature. Wynblatt and Chatain also found the segregation of Au atoms to interfaces in a fcc Pt-1 at.% Au alloy to be higher with increasing grain-boundary energy and higher indexed boundary planes.⁴² Although not explicitly mentioned in their paper, their results implicate that the Au segregation increases with decreasing interfacial coherency. Concerning the influence of dislocations, Choudhury et al⁴⁵ describe a distinct segregation of Cr to misfit dislocations at Fe/Y₂O₃ interfaces under oxidizing conditions. In addition, their experiments on YAl_xCr_{1-x}O₃ particles embedded in a

Fe_{0.78}Al_{0.06}Cr_{0.16} matrix revealed Cr to be enriched at low-coherent interfaces with misfit dislocations in contrast with highly coherent defect-free interfaces. The results of Herbig et al⁴⁶ on the anisotropic segregation of carbon in ferrite clearly demonstrate that the carbon content at the interfaces increases with misorientation angle ω in the low-angle grain boundary regime ($\omega < 14^\circ$). For high-angle grain boundaries, the data indicate the influence of boundary coherency and misfit dislocations. At $\Sigma 3$ and $\Sigma 5$ boundaries, which represent low-energy interfaces, the carbon excess is significantly lower compared to interfaces deviating from the perfect low Σ orientations and hence include misfit dislocations. This agreement between results from highly diverse materials and the findings presented in this study point out that the underlying principles are not limited to Bi-ZnO compositions. In particular, this implicates that the described mechanism of retaining insoluble, otherwise dewetting elements at interfaces is also adaptable for other material systems.

4 | CONCLUSIONS

Two grain-boundary structures in the piezotronic material ZnO with very different local curvature but macroscopically identical orientation of the polarization vector were contrasted in this study. The chosen orientation was a (000 $\bar{1}$) || (000 $\bar{1}$) ZnO bicrystal with tail-to-tail orientation of the c-axis as this configuration was proven to maximize the change of interfacial potential barrier as a function of compressive stress. The salient findings are of general nature and can be summarized as:

Straight interface:

- Interfacial energy of the pure interface is very low and segregation is not observed. Rather, the dopant, notably bismuth, is found in grain-boundary precipitates only.
- The absence of dopant-related interfacial charge states leads to a linear *I-V* characteristics.

Curved interface:

- The interface is characterized by a low coherency leading to a dislocation network at the grain boundary. The interfacial energy therefore is high and lends itself to lowering by segregation, which has been verified by atomically resolved HAADF-STEM as well as EDS investigations.
- This segregation leads to a varistor-type potential barrier, displaying highly nonlinear *I-V* characteristics.

ACKNOWLEDGMENTS

This work was financed by the Deutsche Forschungsgemeinschaft (DFG) under the project numbers KL615/27-1 and RO954/28-1. The authors express

their thanks to Andreas Klein and Phillip Wendel from TU Darmstadt for their support in the RF magnetron sputtering.

ORCID

Maximilian Trapp  <https://orcid.org/0000-0002-4643-204X>

Peter Keil  <https://orcid.org/0000-0002-5197-1224>

Till Frömling  <https://orcid.org/0000-0002-8827-1926>

REFERENCES

- Clarke DR. Varistor ceramics. *J Am Ceram Soc.* 1999;82(3):485–502.
- Blatter G, Greuter F. Carrier transport through grain-boundaries in semiconductors. *Phys Rev B.* 1986;33(6):3952–66.
- Greuter F, Blatter G. Electrical properties of grain boundaries in polycrystalline compound semiconductors. *Semicond Sci Tech.* 1990;5(2):111–37.
- Stucki F, Greuter F. Key role of oxygen at zinc oxide varistor grain boundaries. *Appl Phys Lett.* 1990;57(5):446–8.
- He JL, Liu J, Hu J, Zeng R, Long WC. Non-uniform ageing behavior of individual grain boundaries in ZnO varistor ceramics. *J Eur Ceram Soc.* 2011;31(8):1451–6.
- Hng HH, Knowles KM. Microstructure and current-voltage characteristics of praseodymium-doped zinc oxide varistors containing MnO₂, Sb₂O₃ and Co₃O₄. *J Mater Sci.* 2002;37(6):1143–54.
- Pearnton SJ, Abernathy CR, Overberg ME, Thaler GT, Norton DP, Theodoropoulou N, et al. Wide band gap ferromagnetic semiconductors and oxides. *J Appl Phys.* 2003;93(1):1–13.
- Wang XD, Zhou J, Song JH, Liu J, Xu NS, Wang ZL. Piezoelectric field effect transistor and nanoforce sensor based on a single ZnO nanowire. *Nano Lett.* 2006;6(12):2768–72.
- Wang ZL, Wu WZ. Piezotronics and piezo-phototronics: fundamentals and applications. *Natl Sci Rev.* 2014;1(1):62–90.
- Wen XN, Wu WZ, Pan CF, Hu YF, Yang Q, Wang ZL. Development and progress in piezotronics. *Nano Energy.* 2015;14:276–95.
- Baraki R, Novak N, Hofstätter M, Supancic P, Rödel J, Frömling T. Varistor piezotronics: mechanically tuned conductivity in varistors. *J Appl Phys.* 2015;118(8):085703.
- Keil P, Trapp M, Novak N, Frömling T, Kleebe HJ, Rödel J. Piezotronic tuning of potential barriers in ZnO bicrystals. *Adv Mater.* 2018;30(10):1705573.
- Marks RA, Taylor ST, Mammanna E, Gronsky R, Glaeser AM. Directed assembly of controlled-misorientation bicrystals. *Nat Mater.* 2004;3(10):682–6.
- Hwang JH, Mason TO, Dravid VP. Microanalytical determination of ZnO solidus and liquidus boundaries in the ZnO-Bi₂O₃ system. *J Am Ceram Soc.* 1994;77(6):1499–504.
- Chun SY, Wakiya N, Funakubo H, Shinozaki K, Mizutani N. Phase diagram and microstructure in the ZnO-Pr₂O₃ system. *J Am Ceram Soc.* 1997;80(4):995–8.
- Clarke DR. Grain-boundary segregation in a commercial ZnO-based varistor. *J Appl Phys.* 1979;50(11):6829–32.
- Kingery WD, Sande JBV, Mitamura T. A scanning transmission electron microscopy investigation of grain-boundary segregation in a ZnO-Bi₂O₃ varistor. *J Am Ceram Soc.* 1979;62(3–4):221–2.
- Takemura T, Kobayashi M, Takada Y, Sato K. Effects of bismuth sesquioxide on the characteristics of ZnO varistors. *J Am Ceram Soc.* 1986;69(5):430–6.
- Sato Y, Yamamoto T, Ikuhara Y. Atomic structures and electrical properties of ZnO grain boundaries. *J Am Ceram Soc.* 2007;90(2):337–57.
- Sato Y, Roh JY, Ikuhara Y. Grain-boundary structural transformation induced by geometry and chemistry. *Phys Rev B.* 2013;87(14):140101.
- Sato Y, Yodogawa M, Yamamoto T, Shibata N, Ikuhara Y. Dopant-segregation-controlled ZnO single-grain-boundary varistors. *Appl Phys Lett.* 2005;86(15):152112.
- Ikuhara Y, Pirouz P. Orientation relationship in large mismatched bicrystals and coincidence of reciprocal lattice points (CRLP). *Mater Sci Forum.* 1996;207–209:121–4.
- Wunderlich W. Atomic structure of symmetrical tilt grain boundaries in zinc oxide with high coincidence. *Phys Status Solidi A.* 1998;170(1):99–111.
- Wolf D, Yip S. *Materials interfaces: atomic-level structure and properties.* 1st ed. London: Chapman & Hall; 1992.
- Sutton AP. Irrational interfaces. *Prog Mater Sci.* 1992;36:167–202.
- Chiang YM, Wang H, Lee JR. HREM and STEM of intergranular films at zinc oxide varistor grain boundaries. *J Microsc.* 1998;191:275–85.
- Grillo V. Quantitative evaluation of strain effects in STEM HAADF contrast. *Microscopie.* 2009;11(1):61–8.
- Liu J, Cowley JM. High-resolution scanning-transmission electron-microscopy. *Ultramicroscopy.* 1993;52(3–4):335–46.
- Williams DB, Carter CB, eds. *Spatial resolution and minimum detection.* In: *Transmission electron microscopy: a textbook for materials science.* 2nd ed. New York, NY: Springer, 2009; p. 663–77.
- Bates CH, White WB, Roy R. Solubility of transition metal oxides in zinc oxide and reflectance spectra of Mn²⁺ and Fe²⁺ in tetrahedral fields. *J Inorg Nucl Chem.* 1966;28(2):397–405.
- Gadalla AM. Compatible phases in the system ZnO-CuO-Cu-Cr₂O₃. *Ind Eng Chem Fund.* 1984;23(4):436–40.
- Zhou WZ, Jefferson DA, Alariofranco M, Thomas JM. Superlattices in ternary oxides derived from Bi₂O₃: new families of ordered phases based on the fluorite structure. *J Phys Chem.* 1987;91(3):512–4.
- Miida R, Tanaka M. A modulated structure in a fluorite-type fast-ion-conductor δ-(Bi₂O₃)_{1-x}(Nb₂O₅)_x. *Jpn J Appl Phys.* 1990;29(6):1132–8.
- Elfving M, Österlund R, Olsson E. Differences in wetting characteristics of Bi₂O₃ polymorphs in ZnO varistor materials. *J Am Ceram Soc.* 2000;83(9):2311–4.
- Smith CS. Some elementary principles of polycrystalline microstructure. *Metall Rev.* 1964;9(1):1–48.
- Lyons JL, Janotti A, Van de Walle CG. Role of Si and Ge as impurities in ZnO. *Phys Rev B.* 2009;80(20):205113.
- Raghu N, Kutty TRN. The influence of dislocations on the non-linearity of ZnO: Cu varistors. *J Mater Sci-Mater Electron.* 1990;1(2):84–6.
- Wang HF, Chiang YM. Thermodynamic stability of intergranular amorphous films in bismuth-doped zinc oxide. *J Am Ceram Soc.* 1998;81(1):89–96.
- Pike G. *Semiconducting polycrystalline ceramics.* In: Swain MV, editor. *Material science and technology.* Weinheim, Germany: VCH, 1994; p. 731–53.
- Einzinger R. Grain junction properties of ZnO varistors. *Appl Surf Sci.* 1979;3(3):390–408.
- Gibbs JW. *The collected works of J. Willard Gibbs.* New York, NY: Longmans, Green and Co.; 1928.

42. Wynblatt P, Chatain D. Anisotropy of segregation at grain boundaries and surfaces. *Metall Mater Trans A*. 2006;37(9):2595–620.
43. Kirchheim R. Reducing grain boundary, dislocation line and vacancy formation energies by solute segregation. I. Theoretical background. *Acta Mater*. 2007;55(15):5129–38.
44. Serena S, De la Rubia MA, Caballero AC, Caballero YA. Thermodynamic study of the rich-Bi₂O₃ region of the Bi₂O₃-ZnO system. *Bol Soc Esp Ceram*. 2006;45(3):150–3.
45. Choudhury S, Aguiar JA, Fluss MJ, Hsiung LL, Misra A, Uberuaga BP. Non-uniform solute segregation at semi-coherent metal/oxide interfaces. *Sci Rep*. 2015;5:13086.
46. Herbig M, Raabe D, Li YJ, Choi P, Zaefferer S, Goto S. Atomic-scale quantification of grain boundary segregation in nanocrystalline material. *Phys Rev Lett*. 2014;112(12):126103.

How to cite this article: Trapp M, Keil P, Frömling T, Rödel J, Kleebe H-J. Segregation and properties at curved vs straight (0001) inversion boundaries in piezotronic ZnO bicrystals. *J Am Ceram Soc*. 2020;103:2817–2827. <https://doi.org/10.1111/jace.16912>